Insights into the interaction of discodermolide and docetaxel with tubulin. Mapping the binding sites of microtubule-stabilizing agents by using an integrated NMR and computational approach.

Angeles Canales[1,2], Javier Rodríguez-Salarichs[1,3], Chiara Trigili[1], Lidia Nieto[1], Claire Coderch[4], José Manuel Andreu[1], Ian Paterson[5], Jesús Jiménez-Barbero[1]* and J. Fernando Díaz[1]*.

[1]Dept. Chemical and Physical Biology, Centro de Investigaciones Biológicas, Consejo Superior de Investigaciones Científicas, Ramiro de Maeztu 9, 28040 Madrid, Spain. [2]Facultad de Ciencias Químicas, Universidad Complutense de Madrid, Avda Complutense s/n 28040 Madrid, Spain [3]Centro de Estudios Avanzados de Cuba. Carretera San Antonio km 1 1/2 , Valle Grande, La Lisa, Ciudad Habana, CP. 17100. Cuba [4]Departamento de Farmacología, Universidad de Alcalá, E-28871 Alcalá de Henares, Madrid, Spain [5]University Chemical Laboratory, University of Cambridge, Lensfield Road, Cambridge, CB2 1EW, United Kingdom.

Corresponding authors J. Fernando Díaz: Phone +34-918373112 ext 4269, Fax: +34915360432 e-mail fer@cib.csic.es. J. Jiménez-Barbero. Phone. +34-918373112 ext 4370, Fax: +34915360432 e-mail jjbarbero@cib.csic.es

Abstract

The binding interactions of two antitumour agents that target the paclitaxel site, docetaxel and discodermolide, to unassembled α/β-tubulin heterodimers and microtubules have been studied using biochemical and NMR techniques. The use of discodermolide as a water-soluble paclitaxel biomimetic and extensive NMR experiments allowed the detection of binding of microtubule-stabilizing agents to unassembled tubulin α/β-heterodimers. The bioactive 3D structures of docetaxel and discodermolide bound to α/β-heterodimers were elucidated and compared to those bound to microtubules, where subtle changes in the conformations of docetaxel in its different bound states were evident. Moreover, the combination of experimental TR-NOE and STD NMR data with CORCEMA-STD calculations indicate that docetaxel and discodermolide target an additional binding site at the pore of the microtubules, which is different from the internal binding site at the lumen previously determined by electron crystallography. Binding to this pore site can then be considered as the first ligand-protein recognition event that takes place in advance of the drug internalization process and interaction with the lumen of the microtubules.

Introduction.

The discovery of natural products that attenuate cell growth by acting as inhibitors of cellular microtubules has resulted in the development of clinically-important drugs in cancer chemotherapy(*1-3*). A particularly valuable class of such antimitotic compounds preferentially binds to assembled microtubules over unassembled tubulin, thus stabilizing the polymer and impairing the dynamics. Through this mechanism of action, the dividing tumour cells become blocked in the G2/M phase of the cell cycle resulting in apoptosis. These microtubule-stabilizing agents (MSAs) can be classified into two groups, depending on their competition for three distinct known microtubule-binding sites. The first group includes paclitaxel and its biomimetics (docetaxel, epothilones, discodermolide, dictyostatin, cyclostreptin, etc.)(*4*). These molecules competitively bind to one or both binding sites present in the lumen (internal site of the tubulin β-subunit) and at the pore of the microtubules (external site, involving the α and β subunits of different heterodimers). It is proposed that these ligands bind to this external site and this facilitates transport to the luminal site. In support of this hypothesis, a fluorescent taxoid (hexaflutax) was able to bind only to the external site on microtubules. It was shown that binding to this pore site was sufficient to induce microtubule assembly(*5*),(*6*). Moreover, the binding of cyclostreptin (a MSA that covalently binds tubulin) with microtubules was characterized by mass spectrometry, showing that this ligand binds to both the inner and the pore sites (*7*).

At present, it is not yet established if microtubule-stabilizing agents that target the paclitaxel binding site bind only to the inner, only to the outer, or to both binding sites. However, their strict 1:1 stoichiometry with respect to the α/β-tubulin heterodimer indicates that binding to both sites is mutually exclusive(*4*,*8-9*). Furthermore, indirect evidence supports the presence of a binding site with moderate affinity for MSAs. It is known that fast kinetics of dissociation in the relaxation time scale are required to observe TR-NOESY signals. As it was possible to obtain strong TR-NOESY signals of docetaxel and discodermolide bound to microtubules(*10*),

it is likely that a binding site with a lower affinity than the luminal binding site is also involved in the recognition of these compounds.

The second group of microtubule-stabilizing agents includes laulimalide and peloruside, which compete for a different binding site that has not yet been fully characterized(*11*,*12*).

Microtubule structure determination both in the presence and in the absence of MSAs remains a challenge for structural biology. The complexity of this system, where different aggregation states of the α/β-heterodimer can coexist in solution, has precluded the crystallization of microtubules. Therefore, only 4 Å resolution X-ray structures of RB3-tubulin complexes are available(*13*). Moreover, only a few drugs that target tubulin have been crystallized with the protein, also leading to relatively limited resolution (3.5 Å) structures(*14*,*15*).

In 1998, Nogales et al. reported the first structural data for tubulin in the presence of a microtubule-stabilizing agent(*16*). The structure of Zn-stabilized tubulin sheets in the presence of paclitaxel was determined by electron crystallography, which enabled the location of the paclitaxel binding site within the tubulin β-subunit, establishing interactions with residues at the H6-H7 loop, H7 helix, B7-H9 M-loop and B9-B10 loop. However, the resolution of the structure precluded the complete characterization of the ligand bound conformation, and additional computational studies were needed to refine the ligand orientation and elucidate the key drug-protein interactions(*17*). Subsequently, Nettles et al. reported the structure of the complex of epothilone A bound to zinc-stabilized tubulin sheets by electron crystallography(*18*). This work confirmed that the binding site of this paclitaxel mimetic was located within the same region of the tubulin β-subunit as the paclitaxel site previously described by Nogales. Despite these findings, the aggregation state of this system (Zn-induced sheets) lacks the interprotofilament interactions present in microtubules and, therefore, the precise mapping of the binding site of taxoids and paclitaxel mimetics to microtubules, as well as a detailed knowledge of the molecular recognition process, remains elusive.

In this context, we have focused on determining the binding modes of docetaxel and discodermolide to microtubules in aqueous solution by using an integrated NMR and computational approach. Since the action of these molecules probably involves a multistep mechanism, with different recognition events, we have also studied the binding of these two paclitaxel mimetics to the non-polymerized tubulin α/β–heterodimer, in order to check if the protein is able to recognize the drugs in this non-aggregated state. Although this event seems to be an essential step for the promotion of microtubule formation from tubulin α/β-heterodimers by MSA(*19*), as far as we know, there is no direct biochemical evidence in support of the binding of paclitaxel and its biomimetics to unassembled tubulin.

In previous work, the use of cyclostreptin, a drug that covalently binds to tubulin, allowed the detection of a weak interaction with non-polymerized tubulin α/β-heterodimers at the external pore site(*7*). This region had been predicted to be the transient location for paclitaxel in its way towards the luminal site(*5,20*). Surprisingly, cyclostreptin was found to bind to polymeric tubulin both at the inner luminal and at the pore site. However, for non-polymerized tubulin α/β-heterodimers, it was only bound to the pore site, thus providing the first direct identification of those residues of the external site present in unassembled tubulin. In contrast, the luminal site has been proposed as the binding site on the basis of docking and INPHARMA analysis of epothilones bound to unpolymerized tubulin(*21*).

Herein, we provide experimental evidence for the binding of docetaxel and discodermolide to unassembled tubulin. These compounds promote tubulin polymerization under conditions in which tubulin itself is not able to undergo assembly, i.e. with GDP bound to the exchangeable site(*8*). These results imply that paclitaxel mimetics not only stabilize the microtubule when it is already formed but also can promote microtubule formation. In this work, two key questions related to the mechanism of recognition and stabilization of tubulin by MSA are addressed: the number and location of the binding sites involved in the drug recognition event by

microtubules, and the characterization of the binding of these MSAs to non-polymerized tubulin.

Results.

Characterization of the binding of the MSAs to non-polymerized states of the protein. Binding of discodermolide to tubulin α/β-heterodimer.

Microtubule-stabilizing agents induce microtubule assembly under conditions in which tubulin itself is unable to assemble (GDP-bound and absence of magnesium). Therefore, it is likely that they bind to unassembled tubulin α/β-heterodimer. In practice, the binding of paclitaxel and docetaxel to tubulin in the absence of Mg^{2+} has been previously studied(*19*), using concentrations up to 10 μM of paclitaxel and 50 μM of docetaxel. However, under these conditions, no binding was detected, indicating that the limit for the dissociation constant should be in the millimolar range. In recent years, structurally novel microtubule-stabilizing agents with better solubility and higher affinity for microtubules, as is the case for discodermolide, have been discovered. Thus, higher concentrations of these ligands can be assayed for tubulin binding. The centrifugation assays indicated that discodermolide cosediments with the non-polymerized tubulin α/β-heterodimer in the absence of Mg^{2+} (conditions in which α/β–tubulin is not polymerized(*22*)). However, given the low binding affinity observed (in the range of 10^4 M^{-1}), it was not possible to reach saturation at the maximum possible ligand concentrations and the stoichiometry of the interaction could not be quantified. Nevertheless, since Scatchard analysis of the data indicates 0.85±0.22 sites, we have assumed a 1:1 stoichiometry for the interaction which results in a binding constant of $2.0\pm0.7 \times 10^4$ M^{-1} (Figure 1).

In order to check the specificity of the process, competition experiments were performed. In particular, discodermolide and epothilone B, at 55 μM concentrations, were incubated, both

separately and together, in D_2O with 45 μM tubulin in 10 mM NaPi, 0.1 mM GTP and pH* 7.0. While 0.35 mol epothilone B and 0.17 mol discodermolide per tubulin mol were found to be bound to tubulin when the ligands were incubated separately, the stoichiometries were reduced to 0.21 and 0.09 respectively when the ligands were incubated together. This result indicates that they compete (at least partially) for the same site. Control repeats in H_2O of the corresponding experiments gave the same results.

Purified tubulin is an unstable protein known to rapidly denature in aqueous solution. D_2O has been reported to stabilize tubulin against deactivation and aggregation(*23*), as well as to stabilize protein assemblies, including microtubules(*24*). In order to determine the oligomerization state of tubulin in our experiments, and to rule out any possible changes due to the presence of D_2O or to ligand binding, samples containing 13 and 45 μM tubulin in 10 mM NaPi, 0.1 mM GTP in D_2O, pH* 7.0, at 25 ºC, were analyzed by sedimentation velocity in an analytical ultracentrifuge. These samples were found to contain over 90% of 5.8 S α/β–tubulin heterodimers, two hours after equilibration in the D_2O buffer. Incubation with 55 μM docetaxel or discodermolide did not induce tubulin α/β-heterodimer aggregation under these experimental conditions. Thus, the non-polymerized state of the tubulin α/β-heterodimer was confirmed.

Conformation of microtubule-stabilizing agents bound to non-polymerized tubulin α/β-heterodimer and microtubules.

The bound conformation of docetaxel and discodermolide to the tubulin α/β-heterodimer was deduced by analysis of the TR-NOESY cross peaks, as shown in Figs 2A and 2B respectively (Expanded versions are shown in Supplementary figures 2 and 3 respectively). Extremely weak NOEs were evident between both aromatic moieties (2-OBz and 3'-Ar), resembling the

results obtained for docetaxel bound to microtubules(*25*). These data indicate that the so-called "polar conformation" is not significantly populated in the bound state.

In contrast, strong NOEs were detected between the 4-OAc methyl group and both aromatic rings. The *tert*-butoxy protons also showed clear NOE contacts with both aromatic rings, although significantly weaker than those detected for the 4-OAc group. Notably, this result contrasts with the observations described for docetaxel when bound to microtubules(*25*). In that case, the NOEs between the *tert*-butoxy and 2-OBz meta protons were significantly stronger than those between the 2-OBz meta protons and the 4-OAc group. The ratio of NOE intensities between the key proton pairs was estimated. Thus, the intensity of the Hmeta 2-OBz (two protons)-*tert*-butoxy (nine protons) cross peak was compared to that between the Hmeta 2-OBz (two protons)-4-OAc (three protons) equivalent. The corresponding ratio clearly changed from 2.1 to 1.3, when the NOESY spectra recorded in the presence of microtubules was compared to that with non-polymerized tubulin α/β-heterodimer. This change in intensity ratio could be correlated with a change in the conformation and thus in the relative orientation of the key pendant groups. Furthermore, the data suggest that the non-polymerized tubulin α/β-heterodimer-bound conformation of docetaxel presents a more open arrangement between the hydrophobic groups (2-OBz and *tert*-butoxy) than that adopted when it is bound to microtubules (Figure 2C).

The analysis of the molecular modeling results permitted the determination of the docetaxel conformation bound to non-polymerized tubulin α/β-heterodimer with the best fit to the NMR data as defined by improper torsion angle values for O-C2-C3´-NBz (ϕ1) and O-C2-C3´-C(Ph) (ϕ2) of 98 and -40º, respectively. In contrast, the corresponding torsion angles are 77 and -80º for the docetaxel conformation bound to microtubules. Therefore, the microtubule bound docetaxel conformation as deduced by NMR is intermediate between the so-called T-paclitaxel geometry, described by Snyder et al.(*17*) (defined by $\phi 1$ 80 and $\phi 2$ -58) and the non-polar

geometry (with improper torsion angles $\phi 1$ 42, $\phi 2$ -85). On the other hand, the docetaxel conformation bound to non-polymerized tubulin α/β-heterodimer approximates closely to the T-paclitaxel conformation(*17*).

In contrast, the REDOR-based paclitaxel conformation(*26*) does not account for the observed NOEs under our experimental conditions, neither for dimeric tubulin, nor for microtubules. The REDOR-based conformation displays the C3´ aromatic ring attached to the amide moiety pointing out to the opposite direction of the taxane ring, far apart from the 2-OBz aromatic ring. This geometry cannot satisfy the observed NOE contacts between *tert*-butoxy and 2-OBz protons.

On the other hand, no significant differences were found between the conformation of discodermolide when bound to non-polymerized tubulin α/β-heterodimer or to microtubules. Thus, for discodermolide, the bound conformation in both states corresponds to that previously described(*10*).

Saturation Transfer Difference (STD) analysis of compounds bound to non-polymerized tubulin α/β-heterodimer and to microtubules.

In order to gain insight into the mechanisms employed by microtubule-stabilizing agents to induce microtubule assembly, the binding of these compounds to non-polymerized tubulin α/β-heterodimer and to microtubules was studied using Saturation Transfer Difference analysis. STD-NMR experiments detect magnetization transfer from a given protein to a bound ligand. Only bound ligands show STD signals and, as in any NOE-type experiment, the observed STD effect depends on the distance between the protein and ligand protons, thus providing a useful tool to detect the ligand epitope and to probe the pharmacophore region. Additionally, STD also depends on the exchange rate, binding affinity, concentrations of ligand and receptor, rotational correlation times, and spectrometer frequency. Binding of docetaxel and

discodermolide to non-polymerized tubulin α/β-heterodimer in D_2O, 10 mM NaPi, 0.1 mM GTP and pH* 7.0 could be easily detected by STD (Figure 3A-B). The addition of an excess of discodermolide to a sample containing tubulin and docetaxel reduced the characteristic STD signals of docetaxel, (the peak at 7.50 ppm for the 3´-Ar protons is shown as example in Figure 3C). This result indicates that they compete, at least partially, for the same binding site, as also deduced from the ultracentrifugation experiments (see above). However, given the difference of more than one order of magnitude between the estimated binding constants for those molecules (ca. $2.0x10^4$ M^{-1} for discodermolide and less than $1x10^3$ M^{-1} for docetaxel (*19*)), an even more drastic decrease of the docetaxel STD signals in the presence of discodermolide would have been expected. This finding suggests the presence of additional binding sites for docetaxel binding (see below for further discussion).

The comparison of the STD profiles of docetaxel bound to unassembled tubulin and to microtubules allowed us to identify those protons which are closer to the protein in each aggregation state of the system. It can be observed (Figure 3D) that the profiles are similar, although not identical. As expected, the absolute value of the detected STD effect on docetaxel protons was higher in the presence of microtubules. This result merely reflects that the ligand is bound to a larger receptor in the case of microtubules. In both cases, the protons with the higher STD values were the aromatic ones of the groups at positions 2 and 3'.

In the case of discodermolide, STD effects have smaller values than the ones for docetaxel. In addition, the effects are quite uniform within the molecule for both microtubules and non-polymerized tubulin α/β-heterodimer samples. The protons with the highest STD effect are H11 and 25-CH_3 in the presence of microtubules and H2, H11 in the case of unassembled tubulin heterodimers.

Modeling of the bioactive conformations in the binding sites.

The NMR data obtained were then employed to model the tubulin-bound conformations of discodermolide and docetaxel. First, docking of the ligands in the luminal binding site (1JFF)(*27*) was performed, as previously described(*10*). The resulting docetaxel binding mode at the luminal site (Figure 4A) was fairly similar to that reported for paclitaxel using electron crystallography, as shown in Figure 4B. The discodermolide binding model involving the luminal binding site has already been described in our previous work (*10*).

Additional docking calculations were also performed for the pore site. Initially, the model described by Magnani and co-workers was employed,(*28*). In this case, two binding modes were found (Figure 5A). In the first one, docetaxel was placed between the tubulin β-subunit, close to the luminal site (β1, following the Magnani nomenclature), and the α-subunit of the next dimer in the protofilament (α2, see Figure 5A, cyan structure). In this case, the location of the binding site was similar to that described by Magnani. However, the binding pose of docetaxel was rather different to that described by Magnani for the paclitaxel analogue Hexaflutax. This discrepancy could be due to the different chemical nature of the ligand side chains at C13 and/or to the different docking protocols employed. Magnani treated paclitaxel as a flexible entity, searching for the best pose with no experimental constraints. In contrast, we considered the experimental NOE-based docetaxel conformation for the docking protocol.

In the second solution, docetaxel was bound in the bottom part of the pore, close to subunits β1 and β4 (see Figure 5A, magenta structure), in a similar location to that described by Freedman *et al*.(*29*) However, as in the former case, the obtained binding pose of the ligand relative to this site was different to that described by Freedman.

Docking of discodermolide to the pore site (the geometries of the bound conformers to non-polymerized tubulin α/β-heterodimers and to microtubules are essentially identical) resulted in

a preference for the ligand to occupy the lower part of the pore (Figure 5B), near subunits β1 and β4, as described above for the second solution found for docetaxel.

Corcema-ST calculations

A) Paclitaxel mimetics bound to microtubules

The theoretical STD profiles of the docking models described above were calculated by using the CORCEMA-ST program and compared to the experimental data. In the case of microtubules, the best fit between the experimental and calculated STD values was obtained when the docking solutions located at the pore site were considered (Figure 5A). For docetaxel, the blue conformer (Figure 5A) provided the best fitting (Figure 6A), with a NRMSD=9.9%. In contrast, the pink structure at the pore (Figure 5A) and the geometries docked at the internal site (Figure 4A) did not satisfactorily reproduce the experimental data (see Figure S1 in the supplementary material. Values of NRMDS=56.5% and NRMSD=42.6% were found, respectively).

In the best binding pose (STD- and trNOESY-based), the *tert*-butoxy group of docetaxel is located in the proximity of the CH_3 groups of the side chains of β1 T220 and β1 T221. In fact, T220 is the nucleophile residue that reacts with cyclostreptin and this peptide is protected for hydrogen/deuterium exchange (HDX) in paclitaxel induced microtubules (*30*). The hydroxyl group at position 7 of docetaxel is engaged in hydrogen bonds with β1 E207 and β1 K176 (also protected from HDX, while the aryl group at the C13 side chain occupies the hydrophobic pocket close to β1 Y210 and to the CH_3 of β1 T223. The benzoyl group of docetaxel is located in the vicinity of the CH_3 of α2 A289.

In the case of discodermolide bound to microtubules, the best fit between the experimental NMR data and the docking solutions (Figure 6B NRMSD = 22.4%) was found for the pore site. In this case, the C11 hydroxyl of discodermolide is engaged in two hydrogen bonds with

residues β1 K216 and β1 F212, while the C7 hydroxyl forms a hydrogen bond with β1 T220. One additional hydrogen bond is established between the β4 V93 backbone carbonyl and the hydroxyl moiety at position 17. Me30 is close to β4 F92, while the carbamate moiety of the ligand forms a hydrogen bond with the backbone carbonyl group of β4 F94. The docked solutions located at the internal site provided a much poorer fit with the STD experimental data, as deduced from the high NRMSD = 61.6%.

Therefore, the combined NMR/docking protocol employed herein provides support for the major binding site of both paclitaxel mimetics docetaxel and discodermolide bound to microtubules to be located at the pore of the microtubules.

B) Paclitaxel mimetics bound to non polymerized tubulin α/β heterodimers.

First, it is important to note that the observed STD signals obtained with unassembled tubulin α/β-heterodimer preparations cannot be due to interactions with the complete pore site. Indeed, this cavity is only present in microtubules since it is formed by interactions of different heterodimers. Therefore, in order to obtain a structural view of the interaction of the paclitaxel mimetics with a partially formed pore, additional docking models were evaluated. The first model employed contained only the β1 subunit. This is the region that provided the best fit between the experimental NMR and the CORCEMA–ST predictions for microtubules, as described above (blue structure, Figure 5A). A second model was also calculated by considering only the β4 subunit, which shows major interactions with the C13 side chain of docetaxel, at the pore site (pink structure, Figure 5A). Additional models of docetaxel and discodermolide bound to tubulin α/β-heterodimer in the internal binding site were also evaluated.

Altogether, the fitting procedures between the experimental data and the CORCEMA–ST calculations were carried out evaluating the three putative binding sites – the internal binding

site, the external semi-site at β1, and the external semi-site at β4. The theoretical STD effects calculated for docetaxel bound at the internal binding site (red thin line in Figure 7A) provided a fair agreement with those experimentally observed in the presence of non-polymerized α/β-tubulin heterodimer, NRMSD=22.1%. However, some protons in this model produced STD values higher than those experimentally observed (*o*-Ar, *m*-Ar, p-Ar and H7). Alternatively, the docking pose at the β1 semi-site also provided a reasonable fit to the observed STD profile for the taxane core protons, NRMSD=25.5% (green thin line in Figure 7A), but failed to reproduce the STD profile of most of the protons at the C13 side chain, including those of the aryl and benzoyl rings. Finally, the calculated STD profile for the partially formed pore site at β4 gave a poor fit with the experimental data, NRMSD=40.16% (Supplementary Figure 1B). Thus, no single solution gave a satisfactory match with all the experimental STD data. In practice, a linear combination between the STD values obtained for the luminal binding site with those obtained from the partially formed pore site at β1 gave the best agreement with the experimental data (NRMSD=16.7% dashed line Figure 7A).

For discodermolide, neither the previously reported docking model at the luminal site, NRMDS=27.6 % (red thin line in Figure 7B) (*10*), nor the partially formed pore bound structures, NRMDS=55.5 % (green thin line in Figure 7B) provided a good fit between the calculated and the experimental STD values. As for docetaxel, a linear combination between the STD profiles calculated for both possible binding poses resulted in the best fit, with a NRMSD= 19.5 %.

Discussion

Although ligand binding to unassembled tubulin is essential for explaining the mode of action of microtubule-stabilizing agents(*4*,*9*,*19*), the unequivocal experimental demonstration of its existence has proved elusive. Indeed, it has only been previously observed by covalent

labeling of the pore site(*7*) employing cyclostreptin. Up to now, the reversible interaction of microtubule-stabilizing agents with α/β-tubulin heterodimer in its non-polymerized state had never been directly observed. In order to stabilize microtubules, it is required that the binding affinity of the compound for the assembled state is much higher than that for the unassembled form, thus displacing the assembly equilibrium towards the polymer. Therefore, the existence of low affinity of MSAs for unassembled α/β-tubulin heterodimers can be predicted. This low affinity precluded the previous detection of binding of MSAs to non-polymerized α/β-tubulin heterodimers using centrifugation techniques(*19*). Notably, in the present work, the use of TR-NOESY and STD experiments with discodermolide as microtubule-stabilizing agent, with higher aqueous solubility, has allowed the first experimental detection of binding to non-polymerized tubulin α/β-heterodimers, as well as the biochemical and structural characterization of the interaction.

Two different binding sites in microtubules have been described for paclitaxel biomimetics, the pore site to which binding of cyclostreptin(*7*) and hexaflutax(*6*) take place, and the internal luminal site, where paclitaxel itself interacts(*16*,*31*). When microtubules are formed, it is expected that paclitaxel and its mimetics should be mostly bound to the high affinity luminal site. In principle, the existence of a very high affinity site precludes the use of ligand-based NMR techniques for monitoring interactions, such as TR-NOESY and STD, due to the requirements of fast dissociation rate of the ligands for these experiments to succeed. Therefore, it is highly probable that the binding events associated with this high affinity luminal site are TR-NOESY- and STD-silent. However, these experiments produced clear-cut NMR signals for discodermolide and docetaxel in the presence of microtubules. Therefore, it seems very likely that the observed TR-NOESY and STD signals arise from an alternative binding event, probably a pre-release conformation. In practice, the best fitting of the experimental STD effects to distinct binding mode geometries was obtained when the interaction of the

ligands to the pore site was considered, suggesting that the experimental NMR signals of paclitaxel mimetics bound to microtubules arise from the ligand that has been just released from the microtubules. This final release step complies with the kinetic requirements of TR-NOESY and STD, because it should be fast enough in the relaxation time scale.

Thus, according to our experimental data, MSAs bind and dissociate from/to microtubules following a two-step mechanism.(*32*) The first binding event is assigned to the binding to the external pore site(*7*), from which the dissociation kinetics is fast(*32*). The second, the slow step, should be the internalization towards the luminal site. Subsequently, in the dissociation process, the events are reversed. The first is the slow step, assigned to the transportation from the internal luminal to the external pore site, while the second fast step corresponds to the release of the ligand to the medium. This mechanism implies that the final release step of MSAs from microtubules takes place from the pore. Alternatively, the two steps involved in binding could be due to a conformational rearrangement of the luminal site, resulting in the release of the ligand by diffusion to the medium through the ends of the microtubule. However, this diffusion process should be expected to be rather slow(*33*,*34*) and, therefore, not compatible with the observed fast release of radioactive paclitaxel and docetaxel from assembled microtubules. It has been demonstrated that this phenomenon occurs within two minutes(*35*) and that the rate limiting step is the first slow step of dissociation.

The analysis of the NMR data has indicated the existence of structural differences in the bioactive conformations of docetaxel when bound to microtubules versus non-polymerized α/β-tubulin heterodimer. The resulting 3D models of the ligand-protein complexes (combining docking and CORCEMA-ST calculations) indicated that H229 of the tubulin β-subunit at the luminal site, which simultaneously interacts with the 2-OBz and the C13 side chain in the internal binding site, and therefore makes them spatially separated (Figure 4), does not play any key role in the recognition process at the pore site. Indeed, the corresponding experimental NOEs between the meta protons of the 2-OBz moiety and the *tert*-butoxy protons

at the C13 side chain are significantly different when the TR-NOESY spectra of docetaxel are recorded in the presence of microtubules or non-polymerized α/β-tubulin heterodimer. Therefore, the combined NMR/modelling data strongly suggest that, when microtubules are employed, it is the pore site that is observed by TR-NOESY and STD.

With this information in hand, there is still the question of the actual site (or sites) that is interacting with docetaxel in non-polymerized α/β-tubulin heterodimers. Thus, the experimental data were analyzed and compared to the predictions of CORCEMA-ST for all the possible binding sites described above. The best fit was obtained when the internal binding site was considered, indicating that this is the most plausible binding site for docetaxel in unassembled tubulin (Figure 4). Nevertheless, the fit between the experimental and predicted data considerably improved when the contribution of the β1 semi-site was additionally considered. In fact, the co-existence of two binding sites is in agreement with the observations of the competition experiments which suggested the existence of two simultaneously binding sites for dimeric tubulin. Thus, at the initial stages of the process, and when no polymer has been yet formed, these paclitaxel mimetics mainly interact at the luminal and β1 binding sites, which then further evolves to form the complete pore binding site.

The results presented in this work have allowed the detection of the interaction of docetaxel and discodermolide with non-polymerized α/β-tubulin heterodimers. The interaction has been biochemically characterized, clarifying the manner in which microtubule-stabilizing agents induce microtubule assembly from α/β -heterodimers. These data show that MSAs play a dual role since they not only stabilize microtubules once they are formed, but also promote tubulin polymerization. In addition, the bioactive conformations and the binding epitopes for docetaxel and discodermolide when bound to non-polymerized α/β -tubulin heterodimers have been determined by NMR. Moreover, the binding epitopes of these compounds when bound to microtubules have been also described by using STD data. CORCEMA-ST calculations were

carried out taking into account the two possible binding sites located at the pore and at the lumen of microtubules to discriminate among the different binding poses. The observed NMR findings can be satisfactorily explained by binding of these MSAs at the pore of the microtubules. The existence of this interaction mode therefore suggests that the recognition process of docetaxel and discodermolide by microtubules takes place following a two step mechanism. First, binding to the pore occurs, and then internalization to the lumen takes place.

Finally, the existence of conformational variations in the bound geometry of docetaxel when bound to microtubules and to non-polymerized tubulin α/β-heterodimers has been shown. These observations suggest that the binding of microtubule-stabilizing agents to the tubulin α/β-heterodimer mainly involves the region where the luminal binding site in microtubules will be located. However, the partially formed pore site also participates in ligand recognition.

Methods

Proteins and ligands

Purified calf brain tubulin and chemicals were obtained as previously described(*8*,*36*). Docetaxel (Taxotere) (Figure 1) was kindly provided by Rhône Poulenc Rorer, Aventis (Schiltigheim, France). Discodermolide (Figure 1) was synthesized as described(*37*). All compounds were diluted in 99.8% D6-DMSO (Merck, Darmstad, Germany) to a final concentration of 20 mM and stored at -20 ºC.

Binding of microtubule-stabilizing agents to non-polymerized tubulin α/β-heterodimers.

The binding of microtubule-stabilizing agents to unassembled tubulin heterodimers was determined by centrifugation. Samples containing 50 µM discodermolide in D_2O containing 10 mM sodium phosphate, 0.1 mM GTP pH*(*38*) 7.0 (or the same buffer in H_2O pH 7.0) were

incubated with increasing concentrations of tubulin up to 40 μM at 25 ºC. The samples were centrifuged at 100.000 rpm in a TLA 100.2 rotor in a Beckman Optima TLX ultracentrifuge for 120 minutes. The upper and lower 500 μl were carefully collected, and the pellets were resuspended in 10 mM sodium phosphate, 0.1 mM GTP buffer pH 7.0, the concentration of tubulin in both parts of the tube and in the pellet were determined spectrophotometrically, using an extinction coefficient of 107000 M^{-1} cm^{-1} at 275 nm, in 10 mM phosphate buffer 1% SDS(*39*), by employing a Thermo Evolution 300 LC spectrophotometer. To 300 μl of each sample, 10 μM docetaxel was added as internal standard. The samples were extracted three times with an excess volume of dichloromethane, dried in vacuum and redissolved in 25 μl of 60% methanol. The amount of discodermolide in the samples was analyzed in an Agilent 1100 HPLC, employing a Zorbax Eclipse XDB-C18 developing a gradient from 60 to 70% methanol in water at 1 ml/min (5 min 60% 15 min gradient 5 min 70%).

Analytical ultracentrifugation.

The oligomerization state of the tubulin samples for the NMR experiments was analyzed by sedimentation velocity in a Beckman Optima XL-I analytical ultracentrifuge (Beckman Coulter, Inc., Fullerton, CA) equipped with interference and absorbance optics, using an An50Ti rotor and double sector cells, at 43,000 or 50,000 rpm, 25 ºC. The differential sedimentation coefficient distributions, *c(s)*, were calculated by least squares boundary modeling of sedimentation velocity data using the program SEDFIT(*40-41*). The weight average sedimentation coefficient values measured in the D_2O buffer at 25 ºC were corrected for solvent composition and temperature to H_2O at 20 ºC, s20w, using SEDNTERP, retrieved from the RASMB server(*42*).

NMR sample preparation and experiments

The samples of the ligands bound to non-polymerized tubulin α/β-heterodimers were prepared in 200 μL NMR tubes using a 300 μM concentration of the desired compound and 10 μM of tubulin in D_2O, 10 mM NaPi, 0.1 mM GTP pH* 7.0. The tubulin samples were prepared by removing sucrose, Mg^{2+}, and H_2O from the storage buffer of a 10 mg sample of frozen tubulin, by chromatography using a Sephadex G-25 medium column (25x0.9 cm) equilibrated in D_2O, 10 mM NaPi, 0.1 mM GTP pH* 7.0. Tubulin was centrifuged for 10 minutes at 50.000 in a TLA120 rotor in an Optima TLX centrifuge to remove aggregates, and its concentration was determined spectrophotometrically by employing an extinction coefficient of 107000 M^{-1} cm^{-1} in 10 mM phosphate buffer containing 1% SDS(*39*). The samples were incubated at 25 ºC for 30 min prior to measurement.

The samples of the ligands bound to microtubules were prepared in 200 μL NMR tubes using a 300 μM concentration of the desired compound and 20 μM of tubulin in D_2O, 10 mM KPi, 0.1 mM GMPCPP, 6 mM $MgCl_2$ pH* 6.7. The tubulin samples were prepared by removing sucrose, Mg^{2+}, and H_2O from the storage buffer of a 20 mg sample of frozen tubulin using a two-step procedure by chromatography in a drained centrifuge column of Sephadex G-25 medium (6x1 cm) equilibrated in D_2O , 10 mM KPi, 10 μM GTP pH* 7.0 in the cold, followed by a second chromatography using another Sephadex G-25 medium column (15x0.9 cm) equilibrated in D_2O, 10 mM KPi, pH* 7.0. Tubulin was centrifuged and its concentration measured as above. Tubulin was diluted to 20 μM and GMPCPP 0.1 mM and 6 mM $MgCl_2$ (final pH* 6.7) added prior to the drug addition. The samples were then incubated at 37 ºC for 30 min prior to measurement.

NMR spectra were then recorded at 298 K (dimeric tubulin samples) or 310 K (polymeric tubulin samples) in D_2O on a Bruker AVANCE 500 MHz spectrometer equipped with a triple-

channel cryoprobe. NOESY(*43*) cross peaks were basically zero at room temperature for both docetaxel and discodermolide, and moderately positive at 310 K for free discodermolide.

For the bound ligands, STD and TR-NOE experiments were performed as described(*44*), using a 30:1 ligand receptor molar ratio for the interaction experiments with non-polymerized tubulin α/β-heterodimers, and employing a 15:1 ligand receptor molar ratio for the interaction experiments with microtubules. STD experiments were performed with 0.5, 1, and 2 s saturation times (by concatenation of 50 ms gaussian pulses separated by 1 ms). TR-NOESY experiments with non-polymerized tubulin α/β-heterodimers were performed with mixing times of 50, 100, 200, 250 and 300 ms. No purging spin lock period to remove the NMR signals of the background macromolecule was employed, since they were basically not observable due to the huge size of the receptor. First, line broadening of the ligand protons was monitored after the addition of the protein. Strong negative NOE cross peaks were observed, in contrast to the free state, indicating binding of the ligands to the non-polymerized tubulin α/β-heterodimer or microtubule preparation. The theoretical analysis of the TR-NOEs of the ligand protons was performed using a full relaxation matrix approach with exchange(*45*) as implemented in the CORCEMA program. Different exchange-rate constants were employed to obtain the optimal match between experimental and theoretical results of the intraresidue cross peaks of the ligands, which has a relatively fixed geometry. Given the protein/ligand ratio, the overall correlation time τ_c for the free state was always set to 0.25 ns, since NOESY cross peaks for the free molecule were essentially zero at room temperature and 500 MHz, and the τ_c for the bound state was set to 60 ns for non-polymerized tubulin α/β-heterodimers (τ_c calculated with HYDROPRO (*46*)).

The theoretical STD effects for ligands bound to non-polymerized tubulin α/β-heterodimers and microtubules were calculated using the CORCEMA-ST program. The overall correlation time τ_c for the free state was always set to 0.25 ns and the average rotational motion

correlation time, τ_c, for the bound state was set to 60 ns for non-polymerized tubulin α/β-heterodimers, and 100 ns for microtubules. An order parameter S^2=0.85 was employed to account for the fast rotation of the methyl groups, as implemented in CORCEMA-ST.

In order to fit the experimental STD effects and TR-NOE intensities, off-rate constants between 100-200000 s^{-1} were tested. Optimal agreement was achieved for k_{off} = 100 s^{-1} in the case of microtubules and a combination of K_{off} = 200000 s^{-1} for the pore semi-site and K_{off} = 125000 s^{-1} for the luminal binding site, in the case of non-polymerized tubulin α/β-heterodimers.

Conformational search of ligands.

The calculations were performed using the MacroModel/Batchmin(*47*) package (version 9.6) and the OPLS2005 all-atom force field as implemented in the program Macromodel 9.6. Bulk water solvation was simulated using MacroModel's generalized Born GB/SA continuum solvent model(*48*). The conformational searches were carried out using the torsional sampling MCMM search method implemented in the Batchmin program, and 20,000 Monte Carlo step runs were performed. Extended non-bonded cutoff distances (a van der Waals cutoff of 8.0 Å and an electrostatic cutoff of 20.0 Å) were used. PR conjugate gradient (PRCG) minimization (2000 steps) was used in the conformational search.

Docking calculations.

Docking of the ligands was performed using the AutoDock 4.0 program(*49*). During an AutoDock 4.0 simulation, multiple Lamarckian Genetic Algorithm runs occurred, each one providing one predicted binding mode, and cluster analysis was performed at the end of the simulation. Atomic coordinates for the ligands were obtained from the NMR data assisted by molecular mechanics calculations (see above). The α/β-tubulin dimer coordinates were

obtained from the Protein Data Bank 1JFF code. Model tetramer coordinates were kindly provided by Prof. M. Botta(*28*).

Grids of probe atom interaction energies and electrostatic potential were generated by the AutoGrid program present in AutoDock 4.0. Grid spacing of 0.375 Å were used. For each calculation, one job of 100 docking runs was performed using a population of 200 individuals and an energy evaluation number of 3×10^6. Autodock structures were minimized by using Macromodel 9.6, by several steps of Polak-Ribière conjugate gradient (PRCG) until the energy gradient become lower than 0.001 kJ $Å^{-1}$ mol^{-1}.

Since the scoring function implemented in the Autodock program was not useful to select a docking pose compatible with the experimental NMR results, a new scoring function was implemented, based on the difference between the experimental and theoretical saturation transfer difference (STD) of each ligand's proton (SF-STD). An in-house script which employs custom-made programs written in Fortran90 (to be published) was used to perform exhaustive file treatment in order to score the docked conformations using the CORCEMA-STD program(*50*) to predict the STD values for a given ligand-receptor complex. Briefly, the output files of Autodock were rebuilt and prepared for CORCEMA-STD analysis. In this way, the structural information required for each ligand-receptor complex was prepared for calculating the theoretical STD. Protein residues located inside a sphere of 8 Å around the ligand were considered for the calculations. Finally, the set of docked conformations was ordered according to the normalized root-mean-square deviation (NRMSD) values calculated between the theoretical and the experimental STD values measured for each proton of the ligand.

Acknowledgments.

We wish to thank Dr. C. Alfonso for technical assistance with the analytical ultracentrifugation measurements, Prof. M. Botta for making the pore site coordinates available. We also thank Rhône Poulenc Rorer Aventis for supplying the docetaxel and Matadero Municipal Vicente de

Lucas de Segovia for providing the calf brains for tubulin purification. This work was supported in part by grant BIO2010-16351 and BQU2009-08536 from MICINN (to JFD and JJB respectively), BIPPED-CM from Comunidad de Madrid (JFD, JJB and JMA), EPSRC (IP). We also thank CESGA and the CAI NMR of Universidad Complutense for providing access to their facilities.

References

1. Cragg, G. M., Kingston, D. G., and Newman, D. J. (2005) *Anticancer Agents from Natural Products*, Taylor & Francis, Boca Raton.
2. Paterson, I., and Anderson, E. A. (2005) Chemistry. The renaissance of natural products as drug candidates, *Science 310*, 451-453.
3. Cragg, G. M., Grothaus, P. G., and Newman, D. J. (2009) Impact of Natural Products on Developing New Anti-Cancer Agents, *Chem Rev 109*, 3012-3043.
4. Buey, R. M., Barasoain, I., Jackson, E., Meyer, A., Giannakakou, P., Paterson, I., Mooberry, S., Andreu, J. M., and Díaz, J. F. (2005) Microtubule interactions with chemically diverse stabilizing agents: Thermodynamics of binding to the paclitaxel site predicts cytotoxicity., *Chem Biol 12*, 1269-1279.
5. Díaz, J. F., Barasoain, I., Souto, A. A., Amat-Guerri, F., and Andreu, J. M. (2005) Macromolecular accessibility of fluorescent taxoids bound at a paclitaxel binding site in the microtubule surface, *J Biol Chem 280*, 3928-3937.
6. Barasoain, I., Garcia-Carril, A. M., Matesanz, R., Maccari, G., Trigili, M., Mori, M., Shi, J. Z., Fang, W. S., Andreu, J. M., Botta, M., and Díaz, J. F. (2010) Probing the pore drug binding site of microtubules with fluorescent taxanes: Evidence of two binding poses., *Chem Biol 17*, 243-253.
7. Buey, R. M., Calvo, E., Barasoain, I., Pineda, O., Edler, M. C., Matesanz, R., Cerezo, G., Vanderwal, C. D., Day, B. W., Sorensen, E. J., Lopez, J. A., Andreu, J. M., Hamel,

E., and Díaz, J. F. (2007) Cyclostreptin binds covalently to microtubule pores and lumenal taxoid binding sites, *Nature Chem Biol 3*, 117-125.

8. Díaz, J. F., and Andreu, J. M. (1993) Assembly of purified GDP-tubulin into microtubules induced by taxol and taxotere: reversibility, ligand stoichiometry, and competition, *Biochemistry 32*, 2747-2755.
9. Buey, R. M., Diaz, J. F., Andreu, J. M., O'Brate, A., Giannakakou, P., Nicolaou, K. C., Sasmal, P. K., Ritzen, A., and Namoto, K. (2004) Interaction of Epothilone Analogs with the Paclitaxel Binding Site; Relationship between Binding Affinity, Microtubule Stabilization, and Cytotoxicity, *Chem Biol 11*, 225-236.
10. Canales, A., Matesanz, R., Gardner, N. M., Andreu, J. M., Paterson, I., Diaz, J. F., and Jimenez-Barbero, J. (2008) The Bound Conformation of Microtubule-Stabilizing Agents: NMR Insights into the Bioactive 3D Structure of Discodermolide and Dictyostatin., *Chemistry Eur. J. 14*, 7557-7569.
11. Gaitanos, T. N., Buey, R. M., Díaz, J. F., Northcote, P. T., Teesdale-Spittle, P., Andreu, J. M., and Miller, J. H. (2004) Peloruside A does not bind to the taxoid site on beta-tubulin and retains its activity in multidrug-resistant cell lines, *Cancer Res 64*, 5063-5067.
12. Jiménez-Barbero, J., Canales, A., Northcote, P. T., Buey, R. M., Andreu, J. M., and Díaz, J. F. (2006) NMR determination of the bioactive conformation of peloruside a bound to microtubules, *J Am Chem Soc 128*, 8757-8765.
13. Gigant, B., Curmi, P. A., Martin-Barbey, C., Charbaut, E., Lachkar, S., Lebeau, L., Siavoshian, S., Sobel, A., and Knossow, M. (2000) The 4 A X-ray structure of a tubulin:stathmin-like domain complex, *Cell 102*, 809-816.
14. Ravelli, R. B., Gigant, B., Curmi, P. A., Jourdain, I., Lachkar, S., Sobel, A., and Knossow, M. (2004) Insight into tubulin regulation from a complex with colchicine and a stathmin-like domain, *Nature 428*, 198-202.

15. Gigant, B., Wang, C., Ravelli, R. B., Roussi, F., Steinmetz, M. O., Curmi, P. A., Sobel, A., and Knossow, M. (2005) Structural basis for the regulation of tubulin by vinblastine, *Nature 435*, 519-522.

16. Nogales, E., Whittaker, M., Milligan, R. A., and Downing, K. H. (1999) High-resolution model of the microtubule, *Cell 96*, 79-88.

17. Snyder, J. P., Nettles, J. H., Cornett, B., Downing, K. H., and Nogales, E. (2001) The binding conformation of Taxol in beta-tubulin: A model based on electron crystallographic density, *Proc Natl Acad Sci U S A 98*, 5312-5316.

18. Nettles, J. H., Li, H., Cornett, B., Krahn, J. M., Snyder, J. P., and Downing, K. H. (2004) The binding mode of epothilone A on alpha,beta-tubulin by electron crystallography, *Science 305*, 866-869.

19. Díaz, J. F., Menéndez, M., and Andreu, J. M. (1993) Thermodynamics of ligand-induced assembly of tubulin, *Biochemistry 32*, 10067-10077.

20. Díaz, J. F., Barasoain, I., and Andreu, J. M. (2003) Fast kinetics of Taxol binding to microtubules. Effects of solution variables and microtubule-associated proteins, *J Biol Chem 278*, 8407-8419.

21. Sanchez-Pedregal, V. M., and Griesinger, C. (2009) The Tubulin Binding Mode of MT Stabilizing and Destabilizing., In *Tubulin-Binding Agents. Synthetic, Structural and Mecanistic Insights.* (Carlomagno, T., Ed.), pp 151-208, Springer, Heidelberg.

22. Andreu, J. M., Deancos, J. G., Starling, D., Hodgkinson, J. L., and Bordas, J. (1989) A synchrotron x-ray-scattering characterization of purified tubulin and of its expansion induced by mild detergent binding, *Biochemistry 28*, 4036-4040.

23. Chakrabarti, G., Kim, S., Gupta, M. L., Jr., Barton, J. S., and Himes, R. H. (1999) Stabilization of tubulin by deuterium oxide, *Biochemistry 38*, 3067-3072.

24. Panda, D., Chakrabarti, G., Hudson, J., Pigg, K., Miller, H. P., Wilson, L., and Himes, R. H. (2000) Suppression of microtubule dynamic instability and treadmilling by deuterium oxide, *Biochemistry 39*, 5075-5081.

25. Matesanz, R., Barasoain, I., Yang, C., Wang, L., Li, X., De Ines, C., Coderch, C., Gago, F., Jiménez-Barbero, J., Andreu, J. M., Fang, W., and JF, D. (2008) Optimization of taxane binding to microtubules. Binding affinity decomposition and incremental construction of a high-affinity analogue of paclitaxel, *Chem Biol 15*, 573-585.

26. Geney, R., Sun, L., Pera, P., Bernacki, R. J., Xia, S. J., Horwitz, S. B., Simmerling, C. L., and Ojima, I. (2005) Use of the tubulin bound paclitaxel conformation for structure-based rational drug design, *Chem Biol 12*, 339-348.

27. Nogales, E., Wolf, S. G., and Downing, K. H. (1998) Structure of the alpha beta tubulin dimer by electron crystallography, *Nature 391*, 199-203.

28. Magnani, M., Maccari, G., Andreu, J. M., Diaz, J. F., and Botta, M. (2009) Possible binding site for paclitaxel at microtubule pores, *FEBS J 276*, 2701-2712.

29. Freedman, H., Huzil, J. T., Luchko, T., Luduena, R. F., and Tuszynski, J. A. (2009) Identification and characterization of an intermediate taxol binding site within microtubule nanopores and a mechanism for tubulin isotype binding selectivity, *J Chem Inf Model 49*, 424-436.

30. Xiao, H., Verdier-Pinard, P., Fernandez-Fuentes, N., Burd, B., Angeletti, R., Fiser, A., Horwitz, S. B., and Orr, G. A. (2006) Insights into the mechanism of microtubule stabilization by Taxol, *Proc Natl Acad Sci U S A 103*, 10166-10173.

31. Lowe, J., Li, H., Downing, K. H., and Nogales, E. (2001) Refined structure of alpha beta-tubulin at 3.5 A resolution, *J Mol Biol 313*, 1045-1057.

32. Díaz, J. F., Strobe, R., Engelborghs, Y., Souto, A. A., and Andreu, J. M. (2000) Molecular recognition of taxol by microtubules. Kinetics and thermodynamics of binding of fluorescent taxol derivatives to an exposed site, *J Biol Chem 275*, 26265-26276.

33. Evangelio, J. A., Abal, M., Barasoain, I., Souto, A. A., Lillo, M. P., Acuna, A. U., Amat-Guerri, F., and Andreu, J. M. (1998) Fluorescent taxoids as probes of the microtubule cytoskeleton, *Cell Motil Cytoskeleton 39*, 73-90.

34. Odde, D. (1998) Diffusion inside microtubules, *Eur Biophys J 27*, 514-520.

35. Díaz, J. F., Valpuesta, J. M., Chacón, P., Diakun, G., and Andreu, J. M. (1998) Changes in microtubule protofilament number induced by Taxol binding to an easily accessible site. Internal microtubule dynamics, *J Biol Chem 273*, 33803-33810.

36. Andreu, J. M. (2007) Tubulin Purification, In *Methods in Molecular Medicine* (Zhou, J., Ed.), pp 17-28, Humana Press Inc., Totowa, NJ.

37. Paterson, I., and Lyothier, I. (2004) Total synthesis of (+)-discodermolide: an improved endgame exploiting a Still-Gennari-type olefination with a C1-C8 beta-ketophosphonate fragment, *Org Lett 6*, 4933-4936.

38. Krezel, A., and Bal, W. (2004) A formula for correlating pK(a) values determined in D2O and H2O, *Journal of Inorganic Biochemistry 98*, 161-166.

39. Andreu, J. M., Gorbunoff, M. J., Lee, J. C., and Timasheff, S. N. (1984) Interaction of tubulin with bifunctional colchicine analogues: an equilibrium study, *Biochemistry 23*, 1742-1752.

40. Schuck, P. (2000) Size-distribution analysis of macromolecules by sedimentation velocity ultracentrifugation and lamm equation modeling, *Biophys J 78*, 1606-1619.

41. Schuck, P., Perugini, M. A., Gonzales, N. R., Howlett, G. J., and Schubert, D. (2002) Size-distribution analysis of proteins by analytical ultracentrifugation: strategies and application to model systems, *Biophys J 82*, 1096-1111.

42. Laue, T. M., Shah, B.D., Ridgeway, T.M., Pelletier,S.L. (1992) Computer-aided interpretation of analytical sedimentation data for proteins., In *Analytical Ultracentrifugation in Biochemistry and Polymer Science* (Harding, S. E., Rowe,A.J. and Horton, J.C., Ed.), pp 90-125, Royal Society of Chemistry, Cambridge.

43. Macura, S., and Ernst, R. R. (1980) Elucidation of cross relaxation in liquids by two-dimensional NMR-spectroscopy, *Mol. Phys. 41*, 95-117.

44. Bernardi, A., Potenza, D., Capelli, A. M., García-Herrero, A., Cañada, F. J., and Jiménez-Barbero, J. (2002) Second-generation mimics of ganglioside GM1 oligosaccharide: A three-dimensional view of their interactions with bacterial enterotoxins by NMR and computational methods, *Chem.-Eur. J. 8*, 4598-4612.

45. Moseley, H. N. B., Curto, E. V., and Krishna, N. R. (1995) Complete relaxation and conformational exchange matrix (CORCEMA) analysis of NOESY spectra of interacting systems - 2-dimensional transferred NOESY, *J Mag Reson Ser B 108*, 243-261.

46. Garcia de la Torre, J., Huertas, M. L., and Carrasco, B. (2000) Calculation of hydrodynamic properties of globular proteins from their atomic-level structure, *Biophysical Journal 78*, 719-730.

47. Mohamadi, F., Richards, N. G. J., Guida, W. C., Liskamp, R., Lipton, M., Caufield, C., Chang, G., Hendrickson, T., and Still, W. C. (1990) MacroModel an integrated software system for modeling organic and bioorganic molecules using molecular mechanics., *J. Comput. Chem. 11*, 440-467.

48. Still, W. C., Tempczyk, A., Hawley, R. C., and Hendrickson, T. (1990) Semianalytical treatment of solvation for molecular mechanics and dynamics, *J Am Chem Soc 112*, 6127-6129.

49. Morris, G. M., Goodsell, D. S., Halliday, R. S., Huey, R., Hart, W. E., Belew, R. K., and Olson, A. J. (1998) Automated docking using a Lamarckian genetic algorithm and an empirical binding free energy function, *J Comput Chem 19*, 1639-1662.

50. Jayalakshmi, V., and Krishna, N. R. (2002) Complete relaxation and conformational exchange matrix (CORCEMA) analysis of intermolecular saturation transfer effects in reversibly forming ligand-receptor complexes, *J Magn Reson 155*, 106-118.

Figure Legends

Figure 1.- Chemical structures of docetaxel and discodermolide employed in this study. Scatchard plot of binding of discodermolide to non-polymerized α/β-tubulin heterodimer in 10 mM sodium phosphate, 0.1 mM GTP, pH 7.0 at 25ºC.

Figure 2.- TR-NOESY spectra (mixing time: 300 ms) of the different ligands in the presence of non-polymerized tubulin α/β-heterodimer (D_2O, 298 K) A.- docetaxel and B.- discodermolide. C.- Red colour: docetaxel conformation when bound to microtubules. Blue colour: docetaxel conformation bound to non-polymerized tubulin α/β-heterodimer.

Figure 3.- A.- Off-resonance NMR experiment (500 MHz) (lower line) and STD spectra (upper line) of docetaxel bound to non-polymerized tubulin α/β-heterodimer. B.- Off-resonance NMR experiment (500 MHz) (lower line) and STD spectra (upper line) of discodermolide bound to non-polymerized tubulin α/β-heterodimer. Protons with higher STD are labeled. C.- Decrease of the STD signals of docetaxel with discodermolide concentration. The peak at 7.50 ppm (3´-Aryl protons) is evaluated. D.- Comparison between the STD profiles of docetaxel bound to microtubules (dashed line) and non-polymerized tubulin α/β-heterodimer (solid line).

Figure 4.- A. Docetaxel binding at the luminal binding site. B. Electron crystallography structure of paclitaxel bound to microtubules (pdb code 1JFF).

Figure 5.- A.- Solutions found for the docking of the microtubule bound form of docetaxel into the pore type I of microtubules, the four tubulin heterodimers forming the pore are labeled 1 (grey), 2 (blue) 3 (green) and 4 (orange), docetaxel pose beween heterodimers 1 and 2 is labeled in cyan, while docetaxel pose between heterodimers 1 and 4 is labeled in magenta. B.- Docking of the microtubule bound form of discodermolide into pore type I of microtubules, discodermolide is labeled in light green.

Figure 6.- The comparison between experimental and theoretical STD data (CORCEMA-ST) for docetaxel and discodermolide in the presence of microtubules. A). The experimental STD effects (Solid line and circles) for docetaxel, compared with the calculated ones (dashed line and squares) for this MSA at the pore of microtubules (blue structure, figure 5A). B. The experimental STD effects (solid line and circles) for discodermolide, compared with the calculated ones (dashed line and squares) for this MSA (green structure, figure 5B).

The parameters employed in the CORCEMA calculations were the following; bound correlation time 100 ns, k_{off} 100 s^{-1} and k_{on} 10^8 s^{-1} M^{-1}, for diffusion controlled binding.

Figure 7.- The comparison between experimental and theoretical STD data (CORCEMA-ST) for docetaxel and discodermolide in the presence of non-polymerized tubulin α/β-heterodimers. A). The experimental STD effects (thick line and black circles) for docetaxel compared with the calculated ones for the docking pose at the semi-site at β1 (green circles and thin line, k_{off} 10^5 s^{-1}), and for the docking pose at the luminal site (red circles and thin line, k_{off} 10^5 s^{-1}). The best agreement is found for the combination of these two poses (dashed thick line and black squares) using different k_{off} values of 125000 and 200000 s^{-1}, respectively. B) The experimental STD effects (solid line and circles) for discodermolide when bound to tubulin dimers, compared with the calculated ones when docked at the semi-site at β4 (green circles and thin line) and with those estimated when bound at the luminal site (red circles and thin line). The best agreement is found for the combination of these two poses (dashed thick line and black squares). For discodermolide, the k_{off} values described above were employed for each particular case. All CORCEMA calculations for dimeric tubulin employed a bound correlation time of 60 ns and a k_{on} value of 10^8 s^{-1} M^{-1}, for diffusion-controlled binding.

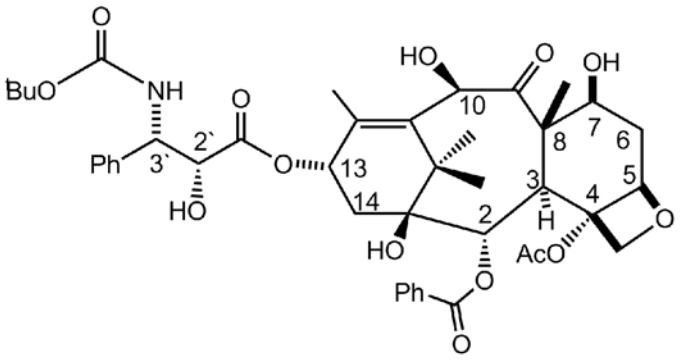

Docetaxel

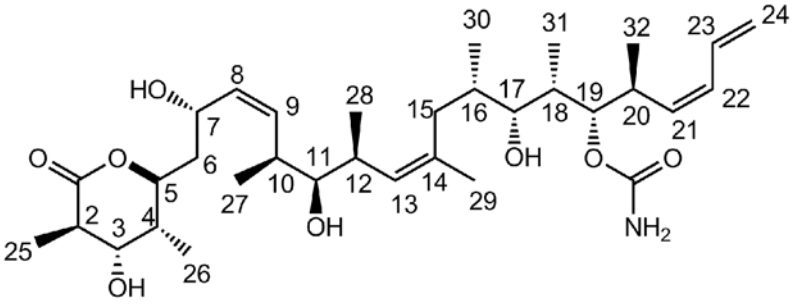

Discodermolide

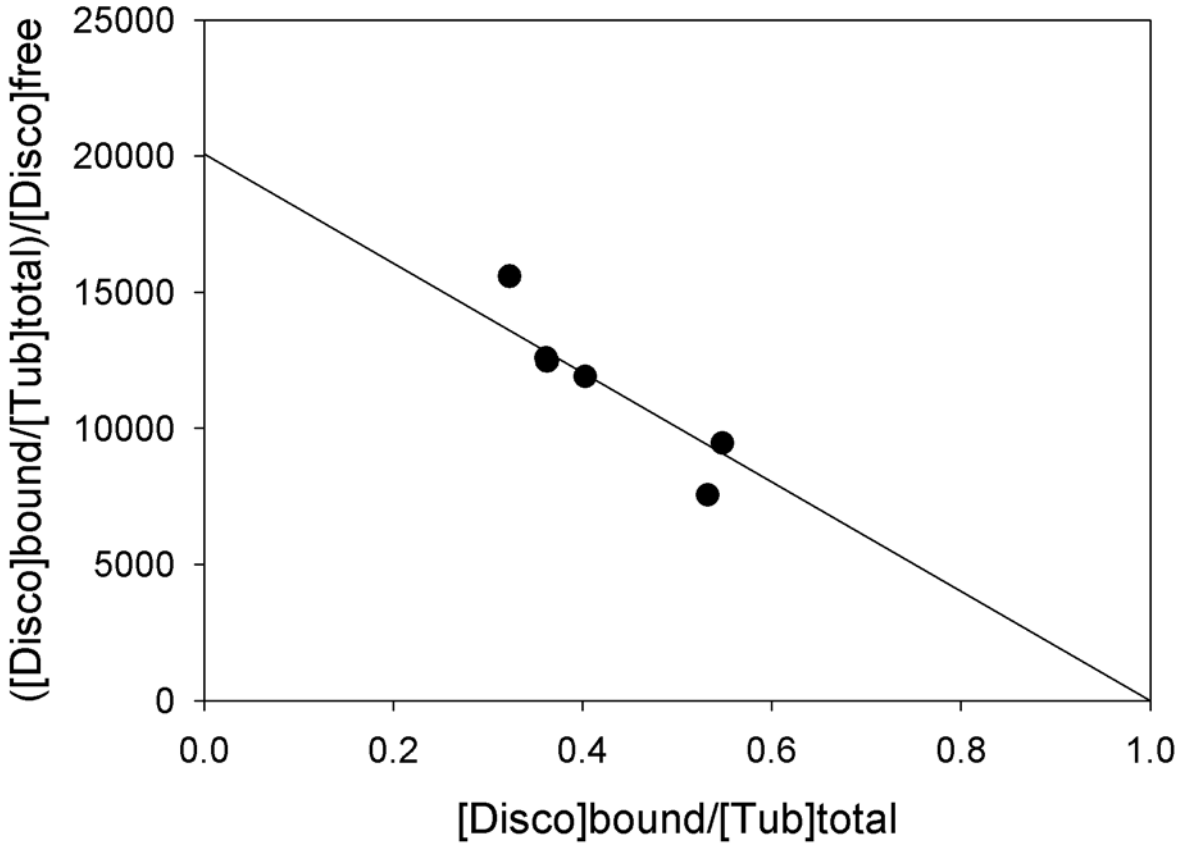

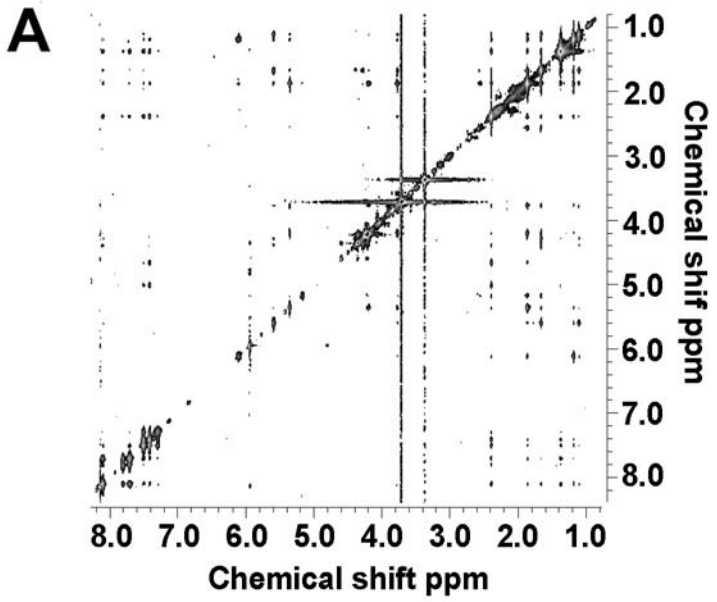
A
1.0
2.0
3.0
4.0
5.0
6.0
7.0
8.0
Chemical shif ppm
8.0 7.0 6.0 5.0 4.0 3.0 2.0 1.0
Chemical shift ppm

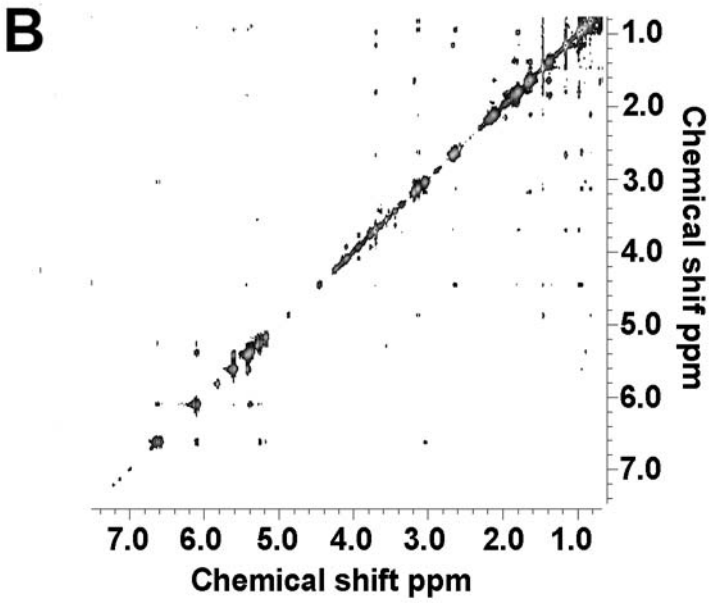
B
1.0
2.0
3.0
4.0
5.0
6.0
7.0
Chemical shif ppm
7.0 6.0 5.0 4.0 3.0 2.0 1.0
Chemical shift ppm

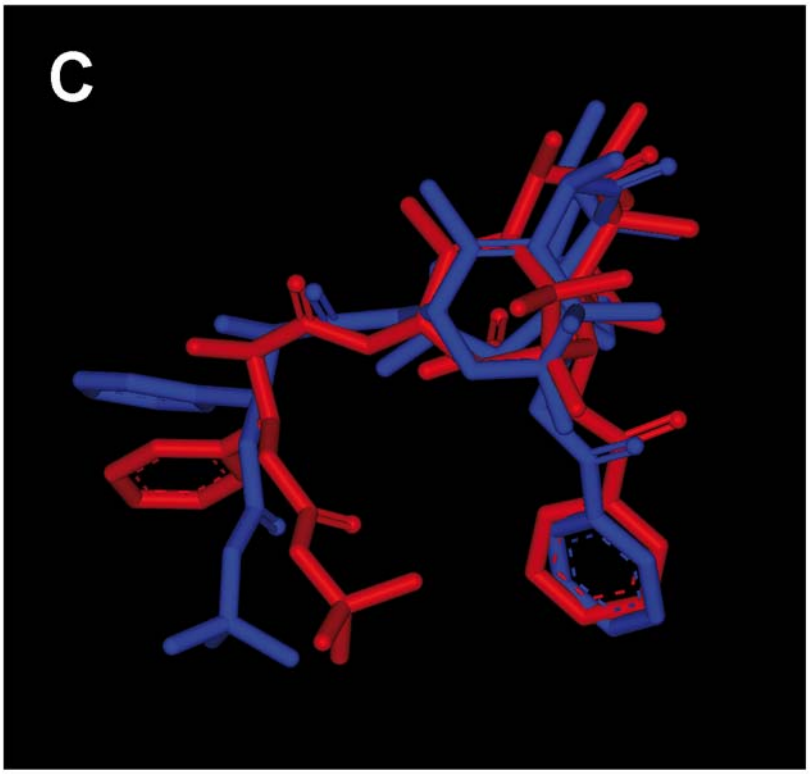
C

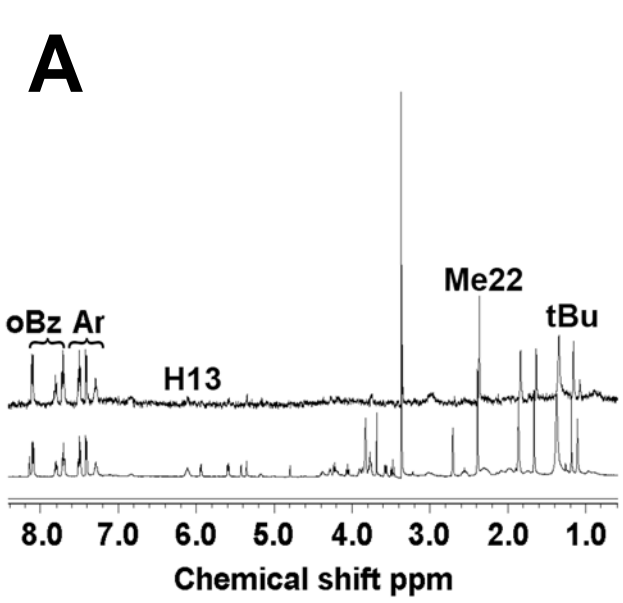
A
oBz Ar
H13
Me22
tBu
8.0 7.0 6.0 5.0 4.0 3.0 2.0 1.0
Chemical shift ppm

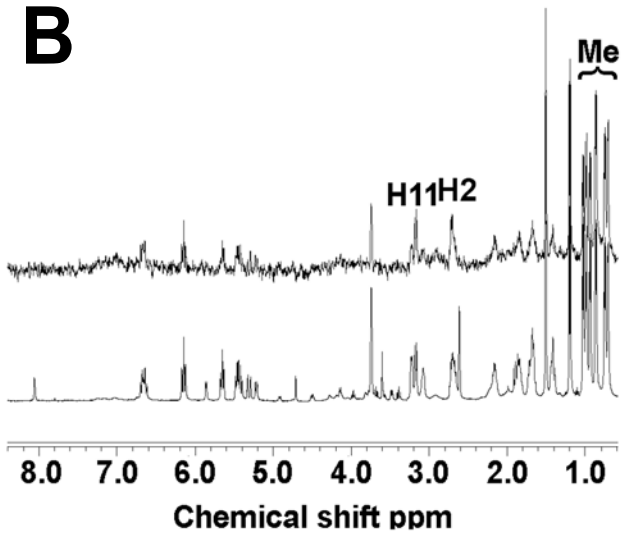
B
H11
H2
Me
8.0 7.0 6.0 5.0 4.0 3.0 2.0 1.0
Chemical shift ppm

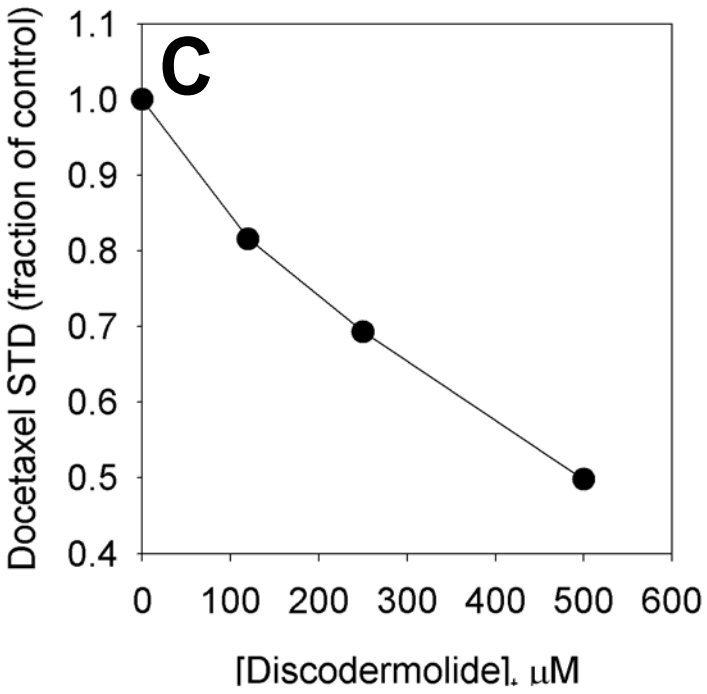
C
Docetaxel STD (fraction of control)
1.1
1.0
0.9
0.8
0.7
0.6
0.5
0.4
0 100 200 300 400 500 600
[Discodermolide], μM

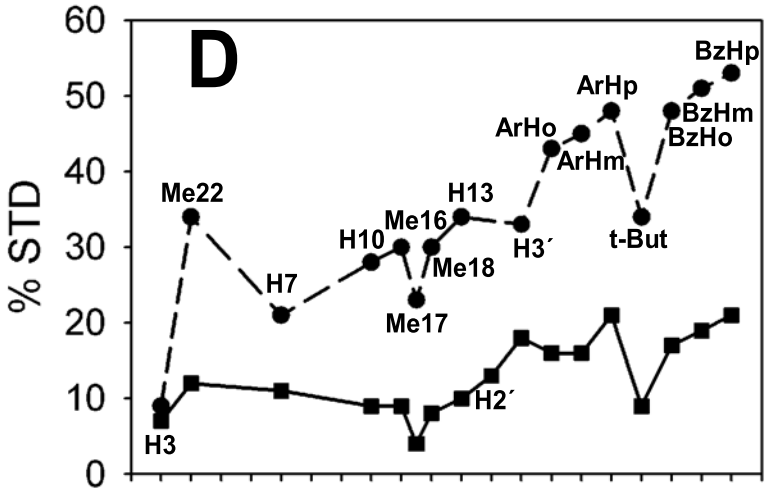
D
% STD
60
50
40
30
20
10
0
Me22
H7
H10
Me16
Me17
Me18
H13
H3´
ArHo
ArHm
ArHp
BzHo
BzHm
BzHp
t-But
H2´
H3

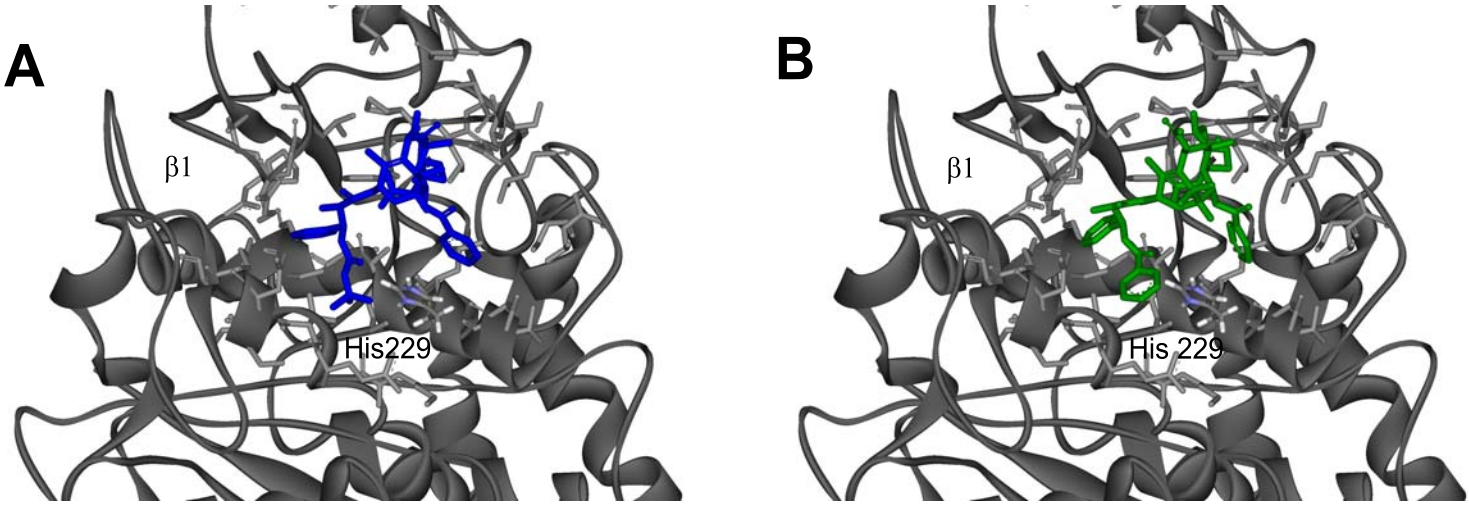
A
β1
His229
B
β1
His 229

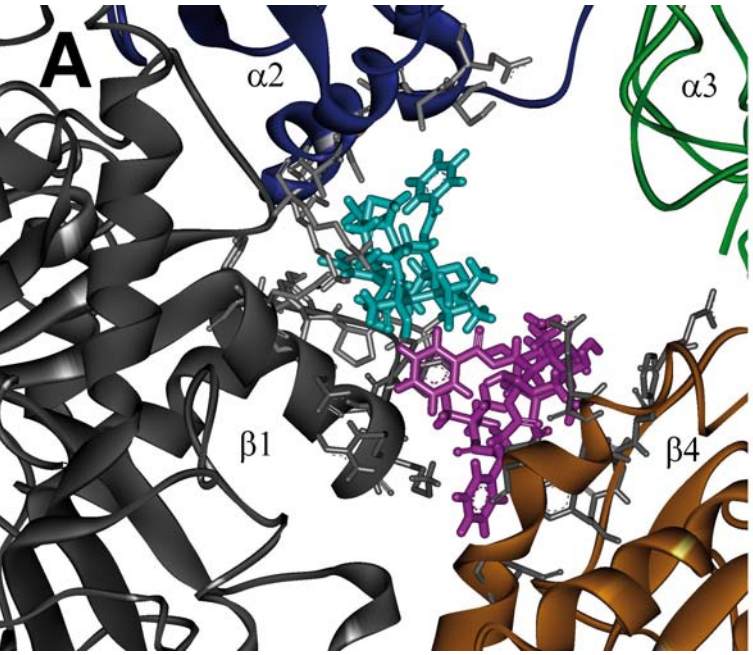
A
α2
α3
β1
β4

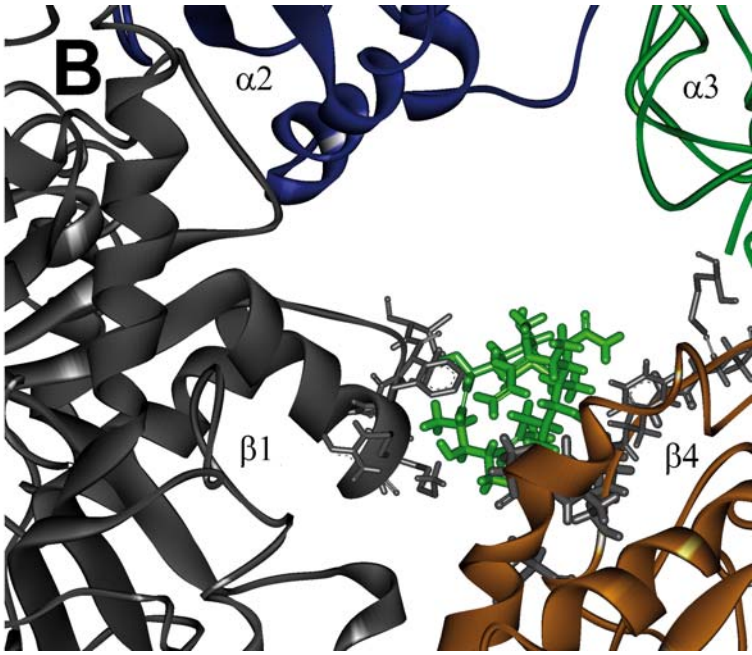
B
α2
α3
β1
β4

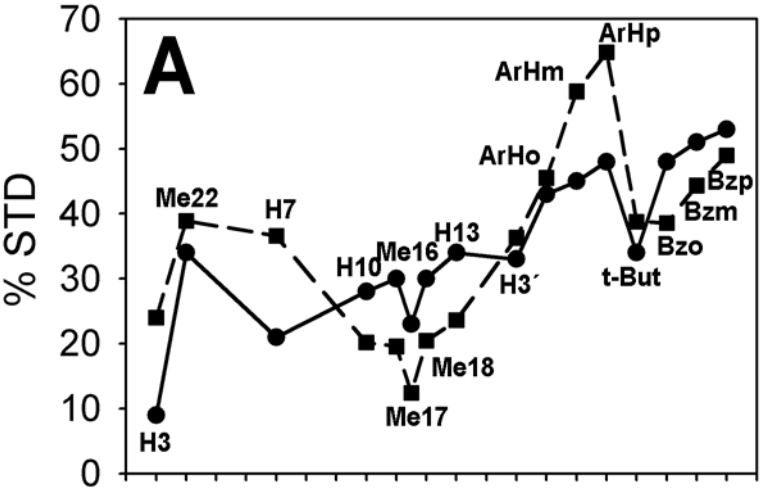
A
% STD
70
60
50
40
30
20
10
0
H3
Me22
H7
H10
Me16
H13
Me17
Me18
H3´
ArHo
ArHm
ArHp
t-But
Bzo
Bzm
Bzp

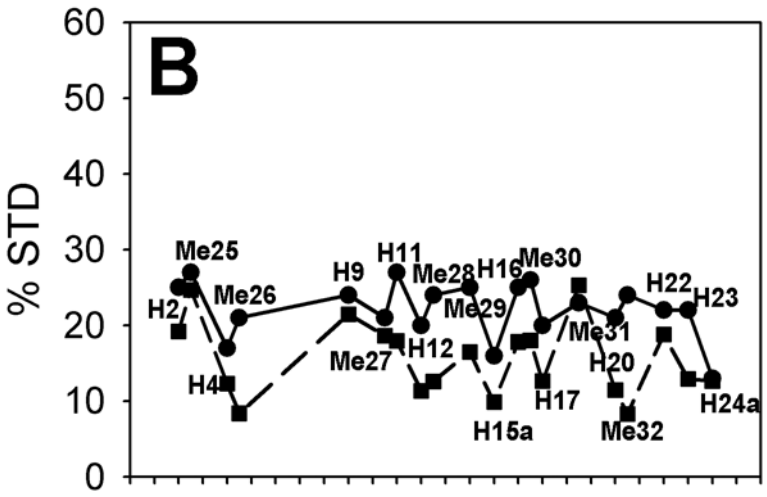
B
% STD
60
50
40
30
20
10
0
H2
Me25
Me26
H4
H9
Me27
H11
H12
Me28
Me29
H16
H15a
Me30
H17
Me31
H20
Me32
H22
H23
H24a

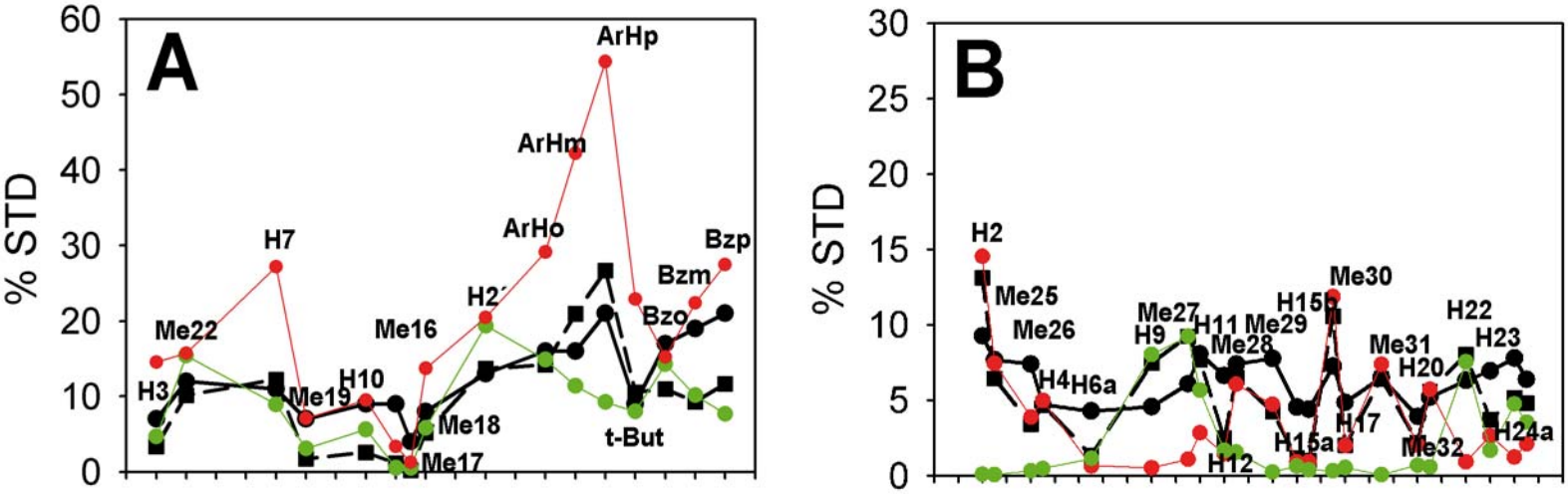
A
% STD
60
50
40
30
20
10
0
ArHp
ArHm
ArHo
H7
H2´
Bzp
Bzm
Bzo
Me22
Me16
H10
H3
Me19
Me18
Me17
t-But
B
% STD
30
25
20
15
10
5
0
H2
Me25
Me26
Me27
H9
H11
Me29
Me28
Me30
H15b
H22
H23
Me31
H20
H4
H6a
H17
H15a
H12
Me32
H24a

Supporting information available:

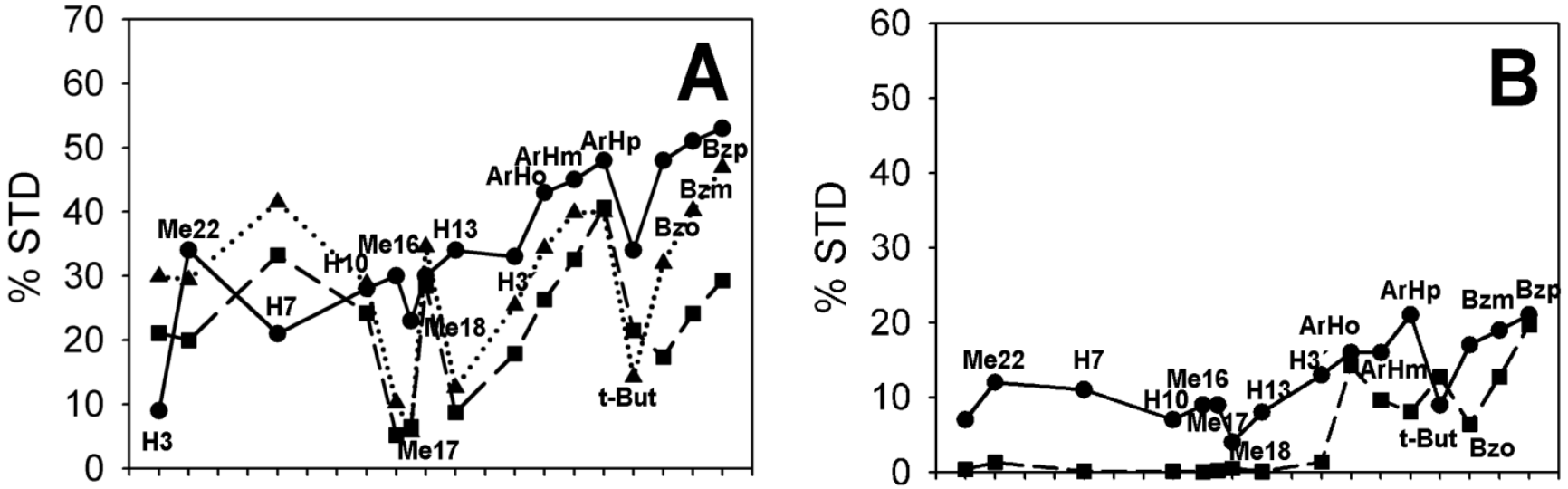

Supplementary Figure 1.- A. Solid line and circles denote docetaxel experimental STD effects when bound to microtubules. Dashed line and squares denote CORCEMA-STD calculation with the coordinates of the docetaxel at the pore of microtubules (pink structure, figure 5A). Dotted line and triangles denote CORCEMA-STD calculation with the coordinates of the docetaxel at the luminal site of microtubules. B. Solid line and circles denote docetaxel experimental STD effects when bound to dimers. Dashed line and squares denote CORCEMA-STD calculation with the coordinates of the docetaxel at the semisite pore (with only β4 present) of microtubules (pink structure, figure 5A).

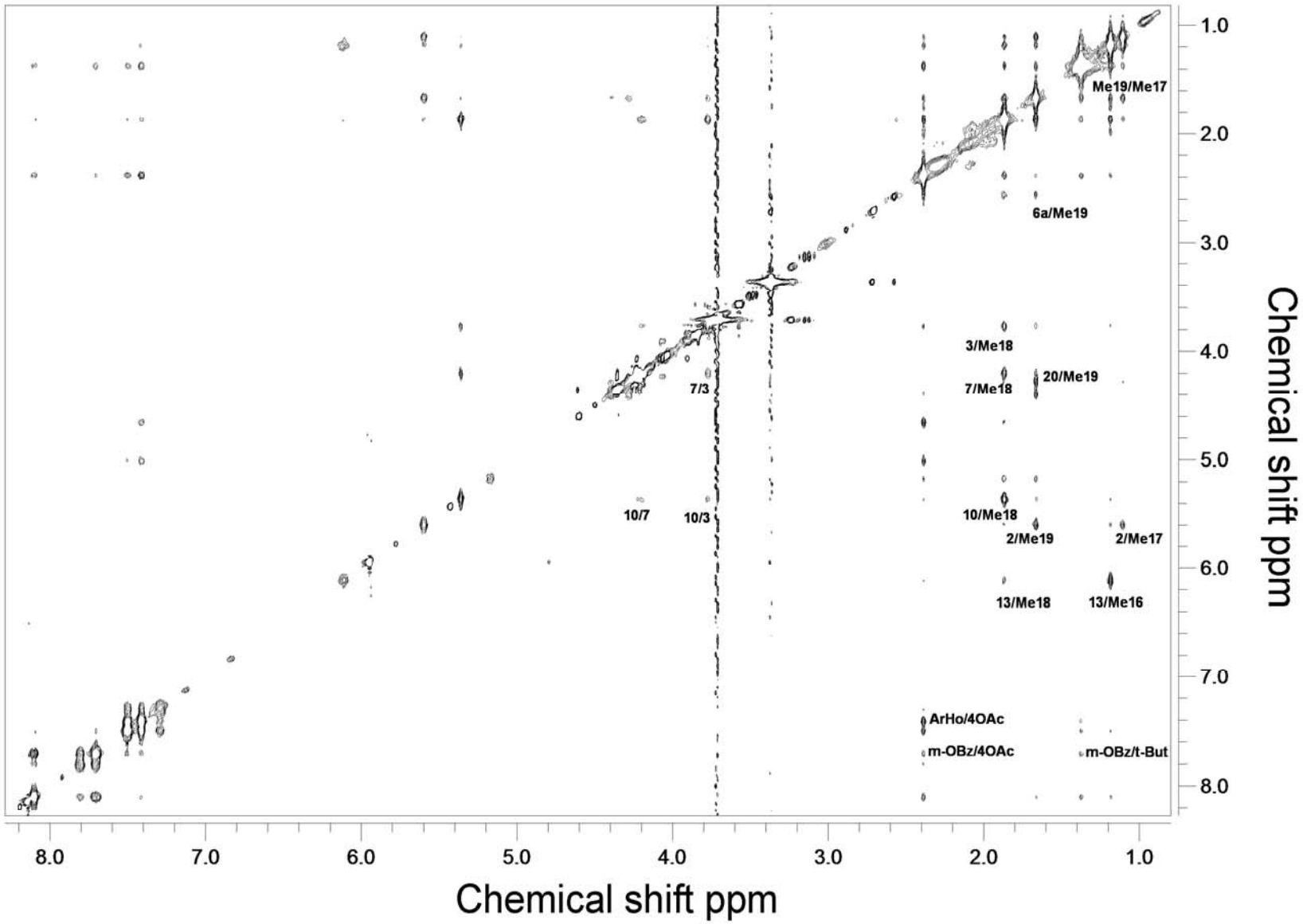

Supplementary figure 2.- Expansion of TR-NOESY spectra (mixing time: 300 ms) of docetaxel (Figure 2A) in the presence of non-polymerized tubulin α/β-heterodimer (D_2O, 298 K).

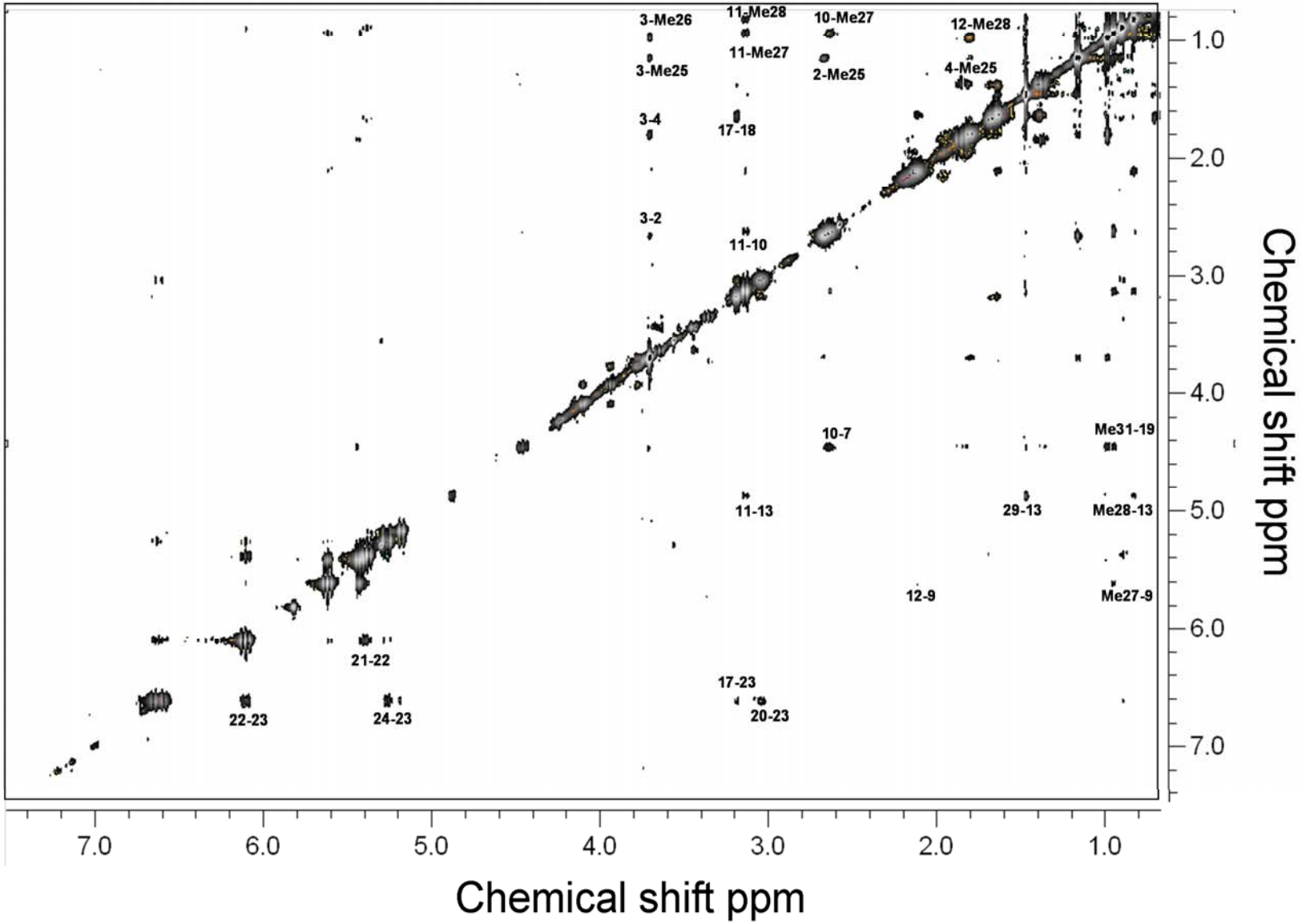

Supplementary figure 3.- Expansion of TR-NOESY spectra (mixing time: 300 ms) of discodermolide (Figure 2B) in the presence of non-polymerized tubulin α/β-heterodimer (D_2O, 298 K).